The merger that led to the formation of the Milky Way's inner stellar halo and thick disk

Helmi, Amina; Babusiaux, Carine; Koppelman, Helmer H.; Massari, Davide; Veljanoski, Jovan; Brown, Anthony G. A.

Published in:
Nature

DOI:
10.1038/s41586-018-0625-x

Publication date:
2018

LETTER

https://doi.org/10.1038/s41586-018-0625-x

The merger that led to the formation of the Milky Way's inner stellar halo and thick disk

Amina Helmi[1]*, Carine Babusiaux[2,3], Helmer H. Koppelman[1], Davide Massari[1], Jovan Veljanoski[1] & Anthony G. A. Brown[4]

The assembly of our Galaxy can be reconstructed using the motions and chemistry of individual stars[1,2]. Chemo-dynamical studies of the stellar halo near the Sun have indicated the presence of multiple components[3], such as streams[4] and clumps[5], as well as correlations between the stars' chemical abundances and orbital parameters[6–8]. Recently, analyses of two large stellar surveys[9,10] revealed the presence of a well populated elemental abundance sequence[7,11], two distinct sequences in the colour–magnitude diagram[12] and a prominent, slightly retrograde kinematic structure[13,14] in the halo near the Sun, which may trace an important accretion event experienced by the Galaxy[15]. However, the link between these observations and their implications for Galactic history is not well understood. Here we report an analysis of the kinematics, chemistry, age and spatial distribution of stars that are mainly linked to two major Galactic components: the thick disk and the stellar halo. We demonstrate that the inner halo is dominated by debris from an object that at infall was slightly more massive than the Small Magellanic Cloud, and which we refer to as Gaia–Enceladus. The stars that originate in Gaia–Enceladus cover nearly the full sky, and their motions reveal the presence of streams and slightly retrograde and elongated trajectories. With an estimated mass ratio of four to one, the merger of the Milky Way with Gaia–Enceladus must have led to the dynamical heating of the precursor of the Galactic thick disk, thus contributing to the formation of this component approximately ten billion years ago. These findings are in line with the results of galaxy formation simulations, which predict that the inner stellar halo should be dominated by debris from only a few massive progenitors[2,16].

The sharp view provided by the second data release (DR2) of the Gaia mission[17] has recently revealed[14] that, besides a few tight streams, a considerable fraction of the halo stars that are near the Sun are associated with a single large kinematic structure. This structure has slightly retrograde mean motion and dominates the blue sequence of the Hertzsprung–Russell diagram (HRD) revealed in the Gaia data[12]. This large structure is readily apparent (in blue) in Fig. 1a, which shows the velocity distribution of stars (presumably belonging to the halo) inside a volume with a radius of 2.5 kpc in the solar vicinity, as obtained from the Gaia data (see Methods for details). Figure 1b shows the velocity distribution from a simulation of the formation of a thick disk via a 20% mass-ratio merger[18]. The similarity between the graphs suggests that the retrograde structure could be largely made up of stars originating in an external galaxy that merged with the Milky Way in the past.

Support for this hypothesis comes from the chemical abundances of stars provided by the APOGEE survey[9]. In Fig. 2a we plot the abundances [α/Fe] and [Fe/H] for a sample of stars cross-matched to Gaia DR2 (see Methods for details). α-elements are produced by massive stars that die fast as supernovae (type II), while iron is also produced in type I supernova explosions of binary stars. Therefore in a galaxy [α/Fe] decreases with time (as [Fe/H] increases). Figure 2a shows the well known sequences defined by the thin and thick disks. The vast majority of the retrograde structure's stars (in blue) follow a well defined separate sequence that extends from low to relatively high [Fe/H]. (The presence of low-α stars with retrograde motions in the halo near the Sun has been reported before[7,19], but for a small sample. The existence of a well populated sequence with lower [α/Fe] was

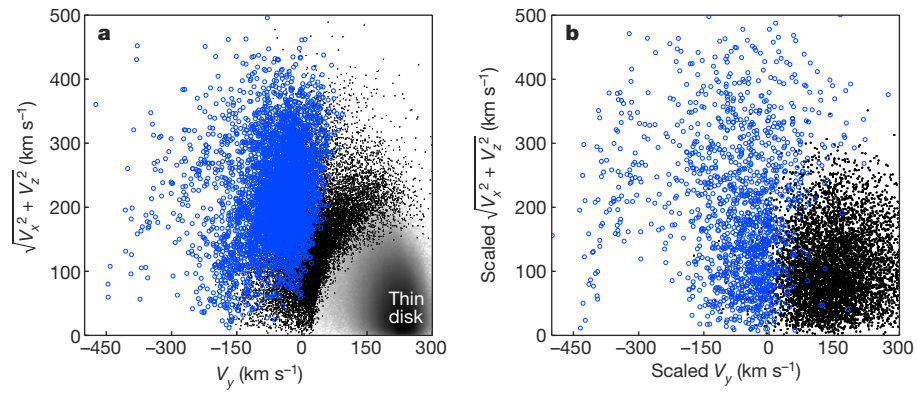

Fig. 1 | Measured velocity distribution of stars in the solar vicinity compared with merger simulation results. a, Velocities of stars in the disk are plotted with grey density contours (because of the large number of stars), and halo stars (selected as those with $|\boldsymbol{V} - \boldsymbol{V}_{\rm LSR}| > 210$ km s^{-1}, where $\boldsymbol{V}_{\rm LSR}$ is the velocity of the local standard of rest) are shown as black points. The blue points are part of a prominent structure with slightly retrograde mean rotational motion and have been selected as those having angular momentum $-1{,}500$ kpc km s$^{-1} < L_z < 150$ kpc km s^{-1} and energy $E > -1.8 \times 10^5$ km^2 s^{-2} (see Methods for details). **b**, Distribution of star particles in a small volume, extracted from a simulation[18] of the formation of a thick disk from the merger of a satellite galaxy (blue symbols) with a pre-existing disk (black points) at a mass ratio of 5:1. The overall morphology of the measured distribution and the observed arch (from $V_y \approx -450$ km s^{-1} and $V_\perp = (V_x^2 + V_z^2)^{1/2} \approx 50$ km s^{-1} to $V_y \approx -150$ km s^{-1} and $V_\perp \approx 300$ km s^{-1} in **a**) can be reproduced qualitatively after appropriately scaling the velocities (see Methods) and by using a simulation with a disk-like satellite (rather than a spherical one, as the arch-like feature is sharper for the disk-like satellite) on a retrograde orbit inclined by about 30°–60°.

[1]Kapteyn Astronomical Institute, University of Groningen, Groningen, The Netherlands. [2]Université Grenoble Alpes, CNRS, IPAG, Grenoble, France. [3]GEPI, Observatoire de Paris, Université PSL, CNRS, Meudon, France. [4]Leiden Observatory, Leiden University, Leiden, The Netherlands. *e-mail: ahelmi@astro.rug.nl

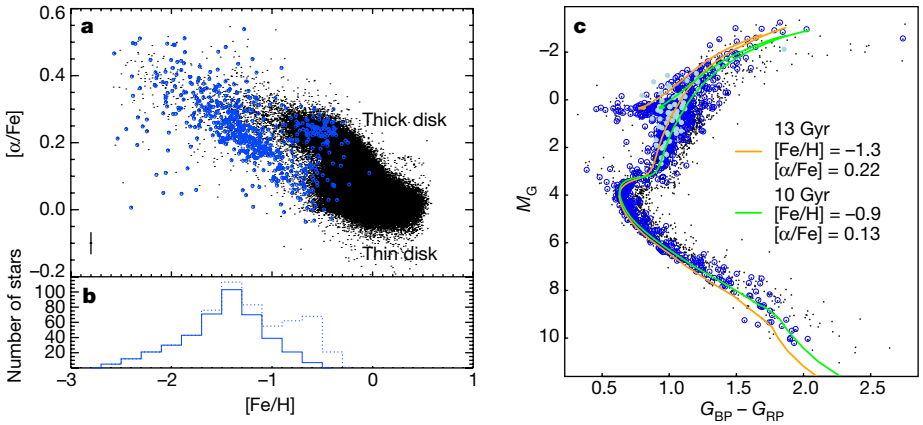

Fig. 2 | Astrophysical properties of stars in Gaia–Enceladus. a, Chemical abundances for a sample of stars located within 5 kpc from the Sun, obtained from cross-matching Gaia and APOGEE data. The blue circles correspond to 590 stars with $-1{,}500$ kpc km s$^{-1} < L_z < 150$ kpc km s^{-1} and energy $E > -1.8 \times 10^5$ km^2 s^{-2} (as in Fig. 1a, but for a larger volume to increase the sample size; see Methods). We note the clear separation between the thick disk and the sequence defined by the majority of the stars in the retrograde structure, except for a small amount of contamination (17%) by thick-disk stars (that is, in the α-rich sequence) that have a similar phase-space distribution to that of the retrograde structure. The error bar in the lower left corner shows the 1σ median error for the sample. **b**, The solid (dotted) histogram shows the metallicity distribution of the retrograde structure without (with) the subset of α-rich stars. The distribution, which peaks at [Fe/H] ≈ -1.6, is reminiscent of the distribution of the stellar halo of the Galaxy[21]. **c**, The HRD for halo stars (black points) selected as in Fig. 1a, with the additional photometric quality cuts[12] of: colour excess $E(B-V) < 0.015$ (to limit its impact on the magnitudes and colours to less than 0.05 mag) and flux excess factor phot-bp-rp-excess-factor $< 1.3 + 0.06(G_{BP} - G_{RP})^2$, where G_{BP} and G_{RP} denote the magnitude in the Gaia BP and RP passband, respectively. M_G is the absolute magnitude in the Gaia G band. In the HRD the blue and red sequences unveiled by Gaia[12] can be seen. Dark-blue symbols represent Gaia–Enceladus stars and light-blue symbols are those that are also in the APOGEE dataset within 5 kpc of the Sun and with [α/Fe] $< -0.14 - 0.35$[Fe/H]. The superimposed isochrones[23] (orange and green lines), which are based on previous work[25], show that an age range of 10–13 Gyr is compatible with the HRD of Gaia–Enceladus.

demonstrated recently using the APOGEE data[11].) An independent analysis[15] has confirmed the relation between the blue sequence in the HRD of the Gaia data and the kinematic structure shown in Fig. 1a and established firmly the link to the low-α stars using both earlier[7] and APOGEE data, thereby making the accretion hypothesis more secure.

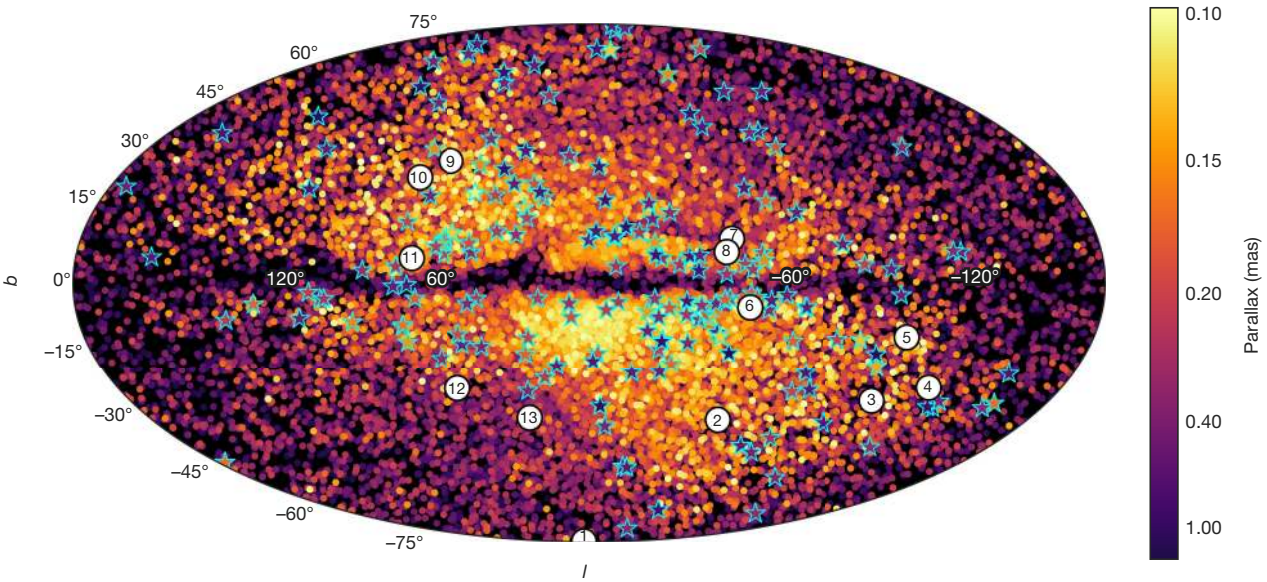

1 NGC 0288 | 3 NGC 1851 | 5 NGC 2298 | 7 ω Cen | 9 NGC 6205 | 11 NGC 6779 | 13 NGC 7099
2 NGC 0362 | 4 NGC 1904 | 6 NGC 4833 | 8 NGC 5286 | 10 NGC 6341 | 12 NGC 7089

Fig. 3 | Sky distribution of candidate Gaia–Enceladus members from a Gaia subsample of stars with full phase-space information. These stars have parallax $\varpi > 0.1$ mas, a relative parallax error of 20% and satisfy the condition $-1{,}500$ kpc km s$^{-1} < L_z < 150$ kpc km s^{-1}. The symbols are colour-coded according to the stars' distance from the Sun (near, dark red; far, light yellow). Because of the large volume explored, we do not include additional selection criteria based on energy, as in Fig. 2 (because the energy depends on the Galactic potential, whose spatial variation across the volume explored is less well constrained than its local value) or on velocity, as in Fig. 1a (because the velocity can vary considerably across this volume). We therefore expect some contamination by thick-disk stars, especially towards the inner Galaxy (see Methods). The star symbols represent Gaia RR Lyrae stars potentially associated with this structure. To identify these, we divide the sky into 128° × 128° bins and log(ϖ) into bins with a width of 0.2 (mimicking the relative parallax error) and measure the average proper motion of Gaia–Enceladus stars in each three-dimensional bin. We then require that the RR Lyrae stars have the same proper motion (within 25 km s^{-1} in each direction at their distance), which corresponds to 1 mas yr^{-1} for stars with $\varpi \approx 0.2$ mas. Globular clusters with $L_z < 50$ kpc km s^{-1}, located between 5 kpc and 15 kpc from the Sun and 40° away from the Galactic centre, are indicated with solid circles. *b*, galactic latitude; *l*, galactic longitude.

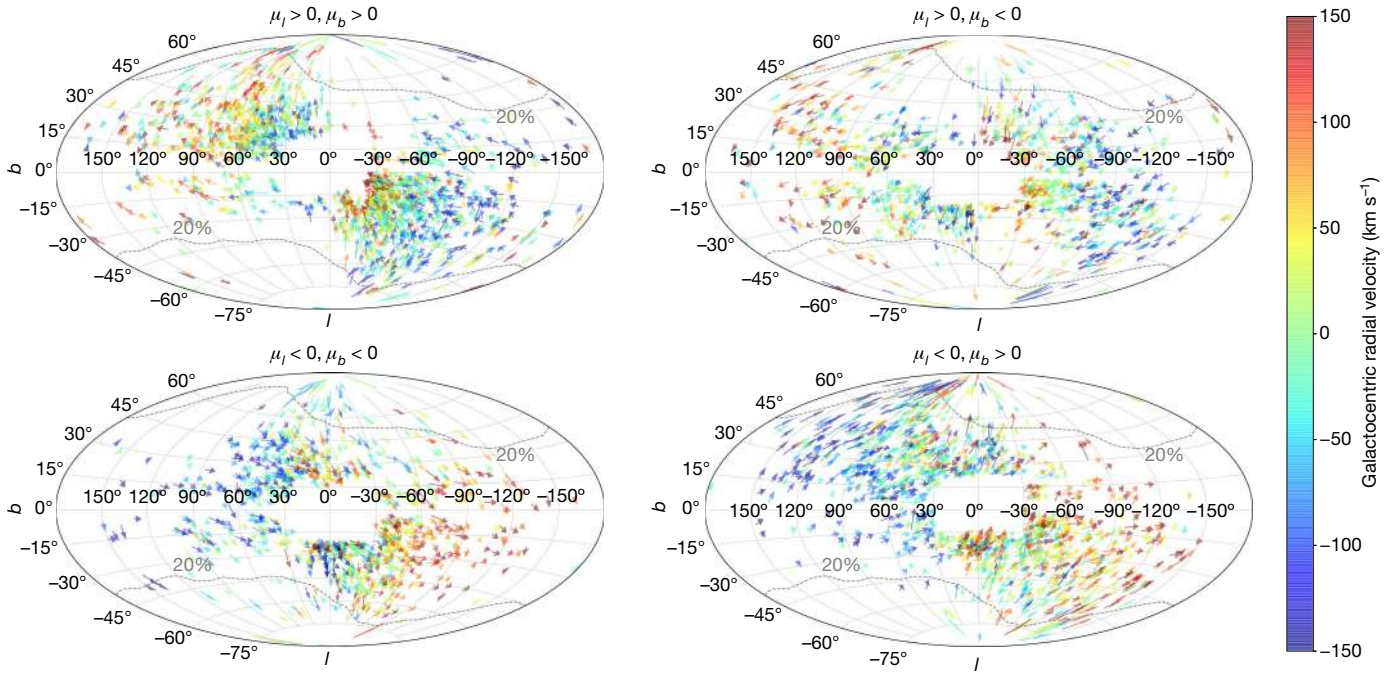

Fig. 4 | Kinematic properties of Gaia–Enceladus candidates. The plotted stars are a subset of those shown in Fig. 3 with 0.1 mas $< \varpi <$ 0.2 mas. The arrows indicate the direction of motion and are colour-coded according to the stars' radial velocity. To avoid cluttering, we show the data in four panels that correspond to different proper-motion ranges and we have removed stars close to the bulge (within 30° in longitude and 20° in latitude). All velocities have been corrected for the solar and local-standard-of-rest motions. The grey contours encompass 90% of the stars in the 6D Gaia dataset that have 0.1 mas $< \varpi <$ 0.2 mas and 20% relative parallax error and clearly demonstrate that the latter selection criterion affects our ability to identify distant Gaia–Enceladus stars in certain regions of the sky. We note the large-scale pattern in the radial velocity, as well as its correlation with the proper-motion component μ_l in the longitude direction: stars with $\mu_l > 0$ (top panels) have $V_{GSR} > 0$ for $l \gtrsim 75°$ and $V_{GSR} < 0$ for $l \lesssim -75°$, where V_{GSR} is the Galactocentric-standard-of-rest velocity, and the reverse occurs for $\mu_l < 0$. Such a global pattern (and its reversal for $-75° \lesssim l \lesssim 75°$) arises because of the coherent retrograde sense of rotation of the stars in their orbits (that is, they have mostly $L_z \lesssim 0$), but the correlation with μ_l is a result of their elongated orbits. For example, we see that if $\mu_l > 0$ and $l \gtrsim 75°$, stars are typically moving outwards away from the Sun at high speed ($V_{GSR} \gtrsim 100$ km s^{-1}).

The large metallicity spread of the stars of the retrograde structure (Fig. 2b) implies that they did not form in a single burst in a low-mass system. Furthermore, the lower [α/Fe] of the more metal-rich stars at the characteristic metallicity of the thick disk ([Fe/H] ≈ −0.6) means that these stars were born in a system with a lower star formation rate than that of the thick disk. The star formation rate required to match the α-poor sequence of the APOGEE data has recently been calculated using a chemical evolution model and including different elemental abundances[20], and it was found to be $0.3 M_\odot$ yr^{-1} and to last for about 2 Gyr ($M_\odot$ is the mass of the Sun). This implies a stellar mass of about $6 \times 10^8 M_\odot$ for the progenitor system. This value is consistent with the large fraction of nearby halo stars that are associated with the structure according to estimates of the local halo density[21] and is comparable to the present-day mass of the Small Magellanic Cloud[22]. Interestingly, previous work[11] has shown that the trends in the abundances of low-metallicity stars in the Large Magellanic Cloud overlap well with the sequence, which implies that the structure was comparable to the Large Magellanic Cloud in its early years. Perhaps more importantly, because [α/Fe] must decrease as [Fe/H] increases, the stars in the structure could not have formed in the same system as the vast majority of stars in the Galactic thick disk. They must have formed, as previously suggested[7,14,15], in a separate galaxy, which we refer to as Gaia–Enceladus (see Methods for the motivation behind the naming).

We now explore whether the Gaia–Enceladus galaxy could have been responsible at least partly for the formation of the thick disk[13–15], as the comparison between the data and the simulation results shown in Fig. 1 suggests. In that case, a pre-existing disk must have been in place at the time of the merger. Figure 2c displays the HRD of the halo stars of Fig. 1a, which shows that the Gaia–Enceladus stars (in blue) populate the blue sequence revealed in the Gaia data[12,14,15]. The thinness of this sequence is compatible with an age range from about 10 Gyr to 13 Gyr, given the stars' abundance sequence, as indicated by the plotted isochrones[23]. Previous studies[24,25], on which this age range is based, have shown that the stars in the α-poor sequence are younger than those in the α-rich sequence for $-1 <$ [Fe/H] < -0.5. This implies that the progenitor of the Galactic thick disk was in place when Gaia–Enceladus fell in, which, according to the ages of its youngest stars, suggests that the merger took place around 10 Gyr ago, that is, at redshift $z \approx 1.8$.

Such a prominent merger must have left debris over a large volume of the Galaxy. To explore where we may find other candidate members of Gaia–Enceladus beyond the solar neighbourhood, we consider stars in the Gaia 6D sample with parallax $\varpi > 0.1$ mas, 20% relative parallax error and a z-direction angular momentum of −1,500 kpc km s$^{-1} < L_z <$ 150 kpc km s^{-1}. Figure 3 shows that nearby candidate Gaia–Enceladus stars (with $\varpi > 0.25$ mas; darker points) are distributed over the whole sky, with this subset being more than 90% statistically complete. More distant stars are preferentially found in specific regions of the sky. Although for such small Gaia parallaxes ($\varpi = 0.1$–0.25 mas) the zero-point offset (about −0.03 mas) is substantial and affects the selection of L_z, it does not affect it to the extent that it can produce the observed asymmetry in the sky. At least in part, this asymmetry is due to the 20% relative parallax error cut, as highlighted in Fig. 4 (see Methods for details and for possible links with known overdensities). In Fig. 3 we have also overplotted (star markers) a subset of 200 Gaia RR Lyrae stars[26]. These have proper motions similar to the mean motion of the candidate Gaia–Enceladus stars, with full phase-space information at their sky position and parallax. Thirteen globular clusters can also be associated with Gaia–Enceladus on the basis of their angular momenta[27] (Fig. 3). All these clusters show a consistent age–metallicity relation[28].

Figure 4 shows the velocity field of the more distant stars associated with Gaia–Enceladus. A large-scale gradient is observed in the radial velocity across the full sky; such a coherent pattern can be obtained

only if stars are moving in the same (retrograde) direction on elongated orbits. The proper motions, depicted by arrows, reveal a complex velocity field. This is expected because of the large mass of the progenitor object and the short mixing timescales in the inner Galaxy[2]. Nonetheless, this complexity contains streams as neighbouring stars often move in the same direction. This is a very significant effect, established by comparing the data with mock sets constructed by assuming a multivariate Gaussian for the velocities (see Methods for details).

We conclude that the halo near the Sun is strongly dominated by a single structure of accreted origin, as also hinted by other work[13,14], and leaves little room for an in situ contribution[15]. This is however not necessarily representative of the whole stellar halo, as debris from other accreted large objects (for example, with different chemical abundance patterns) might dominate elsewhere in the Galaxy. We also conclude that the Milky Way disk experienced a substantial merger in its history. We estimate the mass ratio of this merger at the time that it took place as $M_{\rm h}^{\rm GE}/M_{\rm h}^{\rm MW} = (f^{\rm MW}/f^{\rm GE}) \times (M_*^{\rm GE}/M_*^{\rm MW})$, where f is the ratio of the luminous-to-halo mass of the object, $M_{\rm h}$ and M_* denote the halo mass and stellar mass, respectively, and the superscripts MW and GE represent the Milky Way and Gaia–Enceladus. At the present time, $f^{\rm MW,0} \approx 0.04$ for the Milky Way[29]; if we assume Gaia–Enceladus to be similar to the Large Magellanic Cloud had it evolved in isolation, then[22] $f^{\rm GE,0} \approx 0.01$. It has been shown[30] that the redshift evolution of f between $z = 2$ and $z = 0$ is similar for objects of the scales of the Magellanic Cloud and of the Milky Way, which implies that $f^{\rm MW}/f^{\rm GE} = f^{\rm MW,0}/f^{\rm GE,0} \approx 4$. Therefore, by taking $M_*^{\rm MW}$ at the time of the merger to be the mass of the thick disk[29], that is, $M_*^{\rm MW} \approx 10^{10} M_\odot$, we obtain a mass ratio of about 0.24 for the merger. This implies that the merging of Gaia–Enceladus must have led to considerable heating and to the formation of a thick (or thicker) disk.

Online content

Any methods, additional references, Nature Research reporting summaries, source data, statements of data availability and associated accession codes are available at https://doi.org/10.1038/s41586-018-0625-x.

Received: 15 June 2018; Accepted: 11 September 2018;
Published online 31 October 2018.

1. Freeman, K. & Bland-Hawthorn, J. The new Galaxy: signatures of its formation. *Annu. Rev. Astron. Astrophys.* **40**, 487–537 (2002).
2. Helmi, A., White, S. D. M. & Springel, V. The phase-space structure of cold dark matter haloes: insights into the Galactic halo. *Mon. Not. R. Astron. Soc.* **339**, 834–848 (2003).
3. Carollo, D. et al. Two stellar components in the halo of the Milky Way. *Nature* **450**, 1020–1025 (2007); erratum **451**, 216 (2008).
4. Helmi, A., White, S. D. M., de Zeeuw, P. T. & Zhao, H. Debris streams in the solar neighbourhood as relicts from the formation of the Milky Way. *Nature* **402**, 53–55 (1999).
5. Morrison, H. L. et al. Fashionably late? Building up the Milky Way's inner halo. *Astrophys. J.* **694**, 130–143 (2009).
6. Chiba, M. & Beers, T. C. Kinematics of metal-poor stars in the Galaxy. III. Formation of the stellar halo and thick disk as revealed from a large sample of non-kinematically selected stars. *Astron. J.* **119**, 2843–2865 (2000).
7. Nissen, P. E. & Schuster, W. J. Two distinct halo populations in the solar neighbourhood – evidence from stellar abundance ratios and kinematics. *Astron. Astrophys.* **511**, L10 (2010).
8. Beers, T. C. et al. Bright metal-poor stars from the Hamburg/ESO survey. II. A chemodynamical analysis. *Astrophys. J.* **835**, 81 (2017).
9. Abolfathi, B. et al. The fourteenth data release of the Sloan Digital Sky Survey: first spectroscopic data from the extended Baryon Oscillation Spectroscopic Survey and from the second phase of the Apache Point Observatory Galactic Evolution Experiment. *Astrophys. J. Suppl. Ser.* **235**, 42 (2018).
10. Gaia Collaboration. The Gaia mission. *Astron. Astrophys.* **595**, A1 (2016).
11. Hayes, C. R. et al. Disentangling the Galactic halo with APOGEE. I. Chemical and kinematical investigation of distinct metal-poor populations. *Astrophys. J.* **852**, 49 (2018).
12. Gaia Collaboration. Gaia Data Release 2: observational Hertzsprung–Russell diagrams. *Astron. Astrophys.* **616**, A10 (2018).
13. Belokurov, V., Erkal, D., Evans, N. W., Koposov, S. E. & Deason, A. J. Co-formation of the Galactic disc and the stellar halo. *Mon. Not. R. Astron. Soc.* **478**, 611–619 (2018).
14. Koppelman, H. H., Helmi, A. & Veljanoski, J. One large blob and many streams frosting the nearby stellar halo in Gaia DR2. *Astrophys. J.* **860**, L11 (2018).
15. Haywood, M. et al. In disguise or out of reach: first clues about in-situ and accreted stars in the stellar halo of the Milky Way from Gaia DR2. *Astrophys. J.* **863**, 113 (2018).
16. Cooper, A. P. et al. Galactic stellar haloes in the CDM model. *Mon. Not. R. Astron. Soc.* **406**, 744–766 (2010).
17. Gaia Collaboration. Gaia Data Release 2. Summary of the contents and survey properties. *Astron. Astrophys.* **616**, A1 (2018).
18. Villalobos, A. & Helmi, A. Simulations of minor mergers – I. General properties of thick discs. *Mon. Not. R. Astron. Soc.* **391**, 1806–1827 (2008).
19. Nissen, P. E. & Schuster, W. J. Two distinct halo populations in the solar neighborhood. II. Evidence from stellar abundances of Mn, Cu, Zn, Y, and Ba. *Astron. Astrophys.* **530**, A15 (2011).
20. Fernández-Alvar, E. et al. Disentangling the Galactic halo with APOGEE. II. Chemical and star formation histories for the two distinct populations. *Astrophys. J.* **852**, 50 (2018).
21. Helmi, A. The stellar halo of the Galaxy. *Astron. Astrophys. Rev.* **15**, 145–188 (2008).
22. Van der Marel, R. P., Kallivayalil, N. & Besla, G. Kinematical structure of the Magellanic System. *Proc. IAU* **256**, 81–92 (2008).
23. Marigo, P. et al. A new generation of PARSEC-COLIBRI stellar isochrones including the TP-AGB phase. *Astrophys. J.* **835**, 77 (2017).
24. Schuster, W. J., Moreno, E., Nissen, P. E. & Pichardo, B. Two distinct halo populations in the solar neighborhood. III. Evidence from stellar ages and orbital parameters. *Astron. Astrophys.* **538**, A21 (2012).
25. Hawkins, K., Jofré, P., Gilmore, G. & Masseron, T. On the relative ages of the α-rich and α-poor stellar populations in the Galactic halo. *Mon. Not. R. Astron. Soc.* **445**, 2575–2588 (2014).
26. Clementini, G. et al. Gaia Data Release 2: specific characterisation and validation of all-sky Cepheids and RR Lyrae stars. Preprint at https://arxiv.org/abs/1805.02079 (2018).
27. Gaia Collaboration. Gaia Data Release 2: kinematics of globular clusters and dwarf galaxies around the Milky Way. *Astron. Astrophys.* **616**, A12 (2018).
28. VandenBerg, D. A., Brogaard, K., Leaman, R. & Casagrande, L. The ages of 55 globular clusters as determined using an improved $\Delta V_{\rm TO}^{\rm HB}$ method along with color–magnitude diagram constraints, and their implications for broader issues. *Astrophys. J.* **775**, 134 (2013).
29. McMillan, P. J. The mass distribution and gravitational potential of the Milky Way. *Mon. Not. R. Astron. Soc.* **465**, 76–94 (2017).
30. Behroozi, P. S., Wechsler, R. H. & Conroy, C. The average star formation histories of galaxies in dark matter halos from z = 0–8. *Astrophys. J.* **770**, 57 (2013).

Acknowledgements We are grateful to Á. Villalobos for permission to use his suite of simulations, and to M. Breddels for the software package Vaex (http://vaex.astro.rug.nl), which was used for part of our analyses. We thank H.-W. Rix, D. Hogg and A. Price-Whelan for comments. We have made use of data from the European Space Agency mission Gaia (http://www.cosmos.esa.int/gaia), processed by the Gaia Data Processing and Analysis Consortium (DPAC; see http://www.cosmos.esa.int/web/gaia/dpac/consortium). Funding for DPAC has been provided by national institutions, in particular the institutions participating in the Gaia Multilateral Agreement. We also used data from the APOGEE survey— a part of Sloan Digital Sky Survey IV, which is managed by the Astrophysical Research Consortium for the Participating Institutions of the Sloan Digital Sky Survey (SDSS) Collaboration (http://www.sdss.org). A.H., H.H.K., D.M. and J.V. acknowledge financial support from a Vici grant from the Netherlands Organisation for Scientific Research (NWO) and A.G.A.B. from the Netherlands Research School for Astronomy (NOVA).

Reviewer information *Nature* thanks T. C. Beers, K. V. Johnston and K. Venn for their contribution to the peer review of this work.

Author contributions All the authors contributed to the work. A.H. led and contributed to all aspects of the analysis and wrote the manuscript. C.B. compiled the APOGEE data, provided the cross-match to the Gaia data, was involved in the chemical abundance analysis and, together with D.M., analysed the HRD. H.H.K. and J.V. carried out the dynamical analysis and identification of member stars. A.G.A.B. proposed the preparation of this paper, explored the impact of the selection effects and contributed to the writing of the paper, together with the other co-authors.

Competing interests The authors declare no competing interests.

Additional information
Extended data is available for this paper at https://doi.org/10.1038/s41586-018-0625-x.
Supplementary information is available for this paper at https://doi.org/10.1038/s41586-018-0625-x.
Reprints and permissions information is available at http://www.nature.com/reprints.
Correspondence and requests for materials should be addressed to A.H.
Publisher's note: Springer Nature remains neutral with regard to jurisdictional claims in published maps and institutional affiliations.

METHODS

We describe here the motivation behind the name Gaia–Enceladus. In Greek mythology Enceladus was one of the Giants and the offspring of Gaia (which represents the Earth) and Uranus (which represents the sky). Enceladus was said to be buried under Mount Etna and to be responsible for earthquakes in the region. There are many analogies to the accreted galaxy reported and characterized here, including: (i) being offspring of Gaia and the sky, (ii) having been a 'giant' compared to other past and present satellite galaxies of the Milky Way, (iii) being buried (in reality, first disrupted by the Milky Way and then buried—also in the Gaia data) and (iv) being responsible for seismic activity (that is, shaking the Milky Way and thereby leading to the formation of its thick disk). We refer to the accreted galaxy as Gaia–Enceladus to avoid confusion with one of Saturn's moons, also named Enceladus.

Dataset, selection criteria and the effect of systematics. For this work, we select stars from the Gaia 6D dataset[17] with small relative parallax error $\varpi/\sigma_\varpi > 5$, which allows us to compute their distance from the Sun as $d = 1/\varpi$. For Fig. 1, we consider only stars with $\varpi > 0.4$ mas (that is, within 2.5 kpc from the Sun) to limit the impact of the velocity gradients. The velocities are obtained using the appropriate matrix transformations from the observables α (right ascension), δ (declination), $\mu_{\alpha*}$ and μ_δ (proper motion in the direction of α and δ, respectively) and $V_{\rm los}$ (line-of-sight velocity) and the distances d. These velocities are then corrected for the peculiar motion of the Sun[31] and the local-standard-of-rest-velocity, which is assumed as[29] $V_{\rm LSR} = 232$ km s^{-1}.

We select halo stars (such as the black points in Fig. 1a) as those that satisfy[14] $|\boldsymbol{V} - \boldsymbol{V}_{\rm LSR}| > 210$ km s^{-1}. This condition is used to remove the contribution of the disk(s), although it is less effective towards the inner Galaxy because of the increasing velocity dispersion of disk stars[32]. To select members of the retrograde structure (such as the blue points in Fig. 1a), we inspect the E–L_z distribution of the stars in our dataset. The energy E is computed assuming a Galactic potential including thin-disk, bulge and halo components[33]. For example, Extended Data Fig. 1a shows the E–L_z distribution for all halo stars within 5 kpc from the Sun ($\varpi > 0.2$ mas). Here we have removed stars with phot-bp-rp-excess-factor > 1.27, which is enough to remove some globular cluster stars with poorer photometric quality so as not to apply a colour-dependent correction[34]. This figure shows that the regions occupied by the retrograde structure and by the disk are relatively well separated. There is however some overlap, particularly for higher binding energies and lower angular momenta. Therefore, even the selection criteria $L_z < 150$ kpc km s^{-1} and $E > -1.8 \times 10^5$ km^2 s^{-2} (dashed lines) do not yield a pure (thick-disk-free) sample of stars in the structure. This figure also reveals the large range of energies in the structure, which indicates that member stars are expected over a large range of distances.

Because the energies of stars depend on the gravitational potential of the Galaxy, whose form and amplitude are not so well constrained beyond the solar neighbourhood, we use a criterion based only on L_z to find additional members of the structure/Gaia–Enceladus beyond the immediate vicinity of the Sun (as in Fig. 3). Extended Data Fig. 1b shows the L_z versus the Galactocentric distance R in the disk plane for all stars in the Gaia 6D dataset with $\varpi/\sigma_\varpi > 5$ and parallaxes $\varpi > 0.2$ mas. This plot shows that a selection based only on L_z works relatively well to isolate Gaia–Enceladus stars near the Sun and also farther out in the Galaxy. However, in the inner regions there is much more overlap between the thick disk and Gaia–Enceladus; hence, distinguishing them from each other is less straightforward and the amount of contamination by thick-disk stars is probably much higher. Furthermore, we expect the orbits of some stars in the progenitor of the thick disk to have been perturbed so much during the merger[35] that they 'mingle' with those from Gaia–Enceladus.

Extended Data Fig. 1c shows the z-direction angular momentum as a function of the cylindrical radius of the stellar particles, as obtained from a simulation of the merger of a pre-existing disk and a massive satellite[18,36] (as in Fig. 1b). This example corresponds to the simulation of a disk with mass $M_* = 1.2 \times 10^{10} M_\odot$ and a satellite with mass $M_{*,\rm sat} = 2.4 \times 10^9 M_\odot$ at redshift $z = 1$. Because of the lower host mass used in this simulation (compared to the present-day mass of the Milky Way), the spatial scales and velocities are typically smaller than the data. Therefore, in the simulations we consider as the solar vicinity a volume centred at $R_\odot^{\rm sim} = 2.4 R_{\rm thick}^{\rm final}$, where the final thick-disk scale-length in the simulation is[18] $R_{\rm thick}^{\rm final} = 2.26$ kpc. We also scale the positions by $R_\odot / R_\odot^{\rm sim} = 1.5$ and the velocities by $v_{{\rm thick},\odot}/v_{\rm thick}^{\rm final,sim}$, where $v_{{\rm thick},\odot} = 173$ km s^{-1} is the rotational velocity of the thick disk near the Sun[37] and $v_{\rm thick}^{\rm final,sim}$ is that at $R_\odot^{\rm sim}$ in the simulation. Extended Data Fig. 1c shows that, as in the data, the separation between accreted and host disk stars is less clear for small radii.

For the data of Fig. 2a, we cross-match the catalogues of Gaia DR2 and APOGEE[9,38] DR14 and retain only stars with estimated distances (that is, spectrophotometric and trigonometric parallaxes) that are consistent with each other at the 2σ level. We also require a relative parallax error of 20%. More than 100,000 stars within 5 kpc from the Sun satisfy these conditions. The abundances shown in Fig. 2 are obtained from the ASCAP pipeline[39].

The established presence of a parallax zero-point offset in the Gaia data[40] is partly (if not only) due to a degeneracy between the parallax and the basic-angle variation of the Gaia satellite[41]. Its amplitude varies with the location in the sky[34,40] and is on average −0.029 mas, with a root-mean-square error of about 0.03 mas[27,40]. Such variations make it very difficult to perform a correction a posteriori for the full Gaia DR2 dataset (although the parallax zero-point offset is expected to be smaller than for Gaia DR3). The discovery and characterization of Gaia–Enceladus was done using stars with parallaxes $\varpi > 0.4$ mas in Fig. 1 and for stars with $\varpi > 0.2$ mas from the cross-match of Gaia and APOGEE in Fig. 2. We therefore expect the derived kinematic and dynamical quantities for these subsets to be largely unaffected by the systematic parallax error. However, for Figs. 3, 4, we selected stars on the basis of their L_z, although we focused on properties that are independent of the parallax, such as the position in the sky and proper motions. Nonetheless, to establish how important the parallax zero-point offset is for the selection via L_z, we perform the following test.

We use the Gaia Universe Model Snapshot (GUMS) model v18.0.0[42] and select stars according to the following criteria: apparent magnitude in the Gaia G band $6 \le G \le 13$, surface gravity $0.2 \le \log(g) \le 5$ and effective temperature 3,000 K $\le T_{\rm eff} \le$ 9,000 K. This selection leads to a total of 7,403,454 stars distributed across all Galactic components. For these stars we compute the error-free velocities and L_z and convolve their true parallax with a Gaussian with a dispersion that depends on the magnitude of the star (see https://www.cosmos.esa.int/web/gaia/science-performance, where the end-of-mission uncertainties have been scaled to account for the shorter timespan of DR2). The parallax is reconvolved with a Gaussian with a mean of −0.029 mas and a dispersion of 0.030 mas. Using these observed parallaxes, we compute the 'observed' velocities and L_z.

We find that for measured distances smaller than 5 kpc there is no shift in the derived L_z, whereas for a shell between 5 kpc and 7.5 kpc the median amplitude of the shift is about −50 kpc km s^{-1}, making the observed L_z more retrograde. For a shell between 9 kpc and 10 kpc, the median shift is small and has an amplitude of 20 kpc km s^{-1}, which presumably reflects that at such large distances, random errors dominate in the measurements of individual stars. The results are shown in Extended Data Fig. 2a, where we plot the difference between the true (initial) and 'measured' distributions of L_z for stars 'observed' at distances between 5 kpc and 10 kpc for $l = (-60°, -20°)$. Extended Data Fig. 2b shows the distribution of the mean value of this difference over the whole sky. Although the figure reveals certain patterns, these are different from those seen in Fig. 3. As stated in the main paper, the lack of distant stars in the regions outside the contours of Fig. 4 is the result of a quality cut in the relative parallax error of 20%. This selection criterion allows for parallax errors in the range 0.02–0.04 mas for the most distant stars (with 0.1 mas $< \varpi <$ 0.2 mas); such errors are only reached in those regions of the sky that have been surveyed more frequently by Gaia, such as around the ecliptic poles. The Gaia RR Lyrae stars associated with Gaia–Enceladus also suffer from this effect because a lower number of visits leads to more difficult identification and hence to lower levels of statistical completeness[26].

Random sets and importance of features. To understand how different the dynamical properties of the Gaia 6D dataset are in comparison with a smooth distribution, we plot the distribution of velocities in Extended Data Fig. 3a and of E–L_z in Extended Data Fig. 3b for randomized datasets. These smooth datasets have been obtained from the Gaia data shown in Fig. 1a and in Extended Data Fig. 1a, respectively, by re-shuffling the velocities. That is, to each star, we assign randomly the velocity components V_y and V_z of two other stars in the sample. This results in distributions with the same one-dimensional velocity distributions as the original data, but without any correlations or lumpiness. The comparison of Fig. 1a with Extended Data Fig. 3a shows that the distribution in the random dataset is indeed much smoother than the data and that the overall velocity dispersion in the y direction increases because there is no longer a clear separation between the region occupied by Gaia–Enceladus and by the thick disk. The comparison of Fig. 1b with Extended Data Fig. 3b is even more revealing and clearly shows that the structure defined in E–L_z by Gaia–Enceladus stars has effectively disappeared in the randomized dataset. Similar conclusions are reached when, instead of using a reshuffled dataset, we compare the distributions with those in the GUMS model.

Figure 4 shows the radial velocities and proper motions (corrected for the solar and local-standard-of-rest motions) for stars with 0.1 mas $< \varpi <$ 0.2 mas and −1,500 kpc km s^{-1} $< L_z <$ 150 kpc km s^{-1}. These stars are potential members of Gaia–Enceladus, although, as discussed earlier, contamination by thick-disk stars becomes more important for large distances towards the inner Galaxy. The arrows that depict the proper motions suggest that stars that are close by in the sky move in similar directions. We establish here whether this is statistically significant by comparing the data with a mock dataset.

The mock dataset uses the measured positions of the stars that are plotted in Fig. 4, but with their velocities generated randomly according to a multivariate Gaussian distribution with dispersions of 141, 78 and 94 km s^{-1} in V_R, V_ϕ and V_z, respectively[43], where ϕ is the azimuth angle in the disk plane. During the generation of the mock dataset, we only keep star velocities that satisfy $-1{,}500$ kpc km s^{-1} $< L_z < 150$ kpc km s^{-1}, as in the real data. To quantify the degree of coherence in the proper motions of neighbouring stars in the sky, we perform the following test. For each star, we find its nearest neighbour in the sky and then determine the angle between their proper-motion vectors. We then count the number of such pairs with a given angle. Extended Data Fig. 4 shows the distribution of these pairs for the Gaia subsample (blue) and for the mock dataset (red). There is a clear excess of pairs of stars with similar directions of motion in the data in comparison with the mock dataset.

Context and link with other substructures. Hints of the presence of a population like Gaia–Enceladus have been reported in the literature in the last two decades and have been typically based on small samples of stars. These hints were of a chemo-dynamical nature[6,8,44] and sometimes attributed to accretion[5,45], but also based purely on chemical signatures, such as the α-poor sequence[7,19]. More recently, cross-matches to the first data release of the Gaia mission[46] also revealed the contrast between the metal-rich population, which is supported by prograde rotation and associated with the tail of the thick disk[47], and the metal-poor halo, which we have identified as Gaia–Enceladus. Furthermore, in one study[13] the difference in the kinematics of these two populations, as well as the measurement of a very radially biased velocity ellipsoid for halo stars with [Fe/H] > -1.7, led to the proposal that this population (which was termed 'Gaia sausage') could be the result of a substantial merger. Although this could be also attributed to an in situ formation via a radial collapse, this hypothesis is further supported by the orbits of the stars in the population, leading to a break in the halo density profile at about 20 kpc[48]. All of these pieces of evidence together outline the case for the discovery and detailed characterization of Gaia–Enceladus reported here.

The more distant Gaia–Enceladus debris occupies large portions of the sky that are not extensively covered by other existing surveys. There is however a recent detection of an overdensity identified by the PanSTARRS and the WISE surveys with the help of Gaia proper motions[49], which overlaps with the northern part of the more distant Gaia–Enceladus stars for -2 mas yr^{-1} $< \mu_\alpha < -1$ mas yr^{-1} and -1 mas yr^{-1} $< \mu_\delta < 0$ mas yr^{-1} and partly (but not fully because of the PanSTARRS footprint) with the southern part for 0 mas yr^{-1} $< \mu_\alpha < 1$ mas yr^{-1} and -3 mas yr^{-1} $< \mu_\delta < -1$ mas yr^{-1}. There could be also a relationship with the Hercules Aquila Cloud[50] identified in SDSS data, although this appears to be offset both in the northern and southern hemispheres and is located at a larger distance. The location of intermediate-distance Gaia–Enceladus stars in the sky seems to overlap with the Hercules thick-disk cloud[51], especially in the fourth Galactic quadrant below the Galactic plane.

Data availability

All data generated and analysed in this study are provided as Source Data or Supplementary Data.

31. Schönrich, R., Binney, J. & Dehnen, W. Local kinematics and the local standard of rest. *Mon. Not. R. Astron. Soc.* **403**, 1829–1833 (2010).
32. Gaia Collaboration. Gaia Data Release 2: mapping the Milky Way disc kinematics. *Astron. Astrophys.* **616**, A11 (2018).
33. Helmi, A., Veljanoski, J., Breddels, M. A., Tian, H. & Sales, L. V. A box full of chocolates: the rich structure of the nearby stellar halo revealed by Gaia and RAVE. *Astron. Astrophys.* **598**, A58 (2017).
34. Arenou, F. et al. Gaia Data Release 2: catalogue validation. *Astron. Astrophys.* **616**, A17 (2018).
35. Jean-Baptiste, I. et al. On the kinematic detection of accreted streams in the Gaia era: a cautionary tale. *Astron. Astrophys.* **604**, A106 (2017).
36. Villalobos, A. & Helmi, A. Simulations of minor mergers – II. The phase-space structure of thick discs. *Mon. Not. R. Astron. Soc.* **399**, 166–176 (2009).
37. Morrison, H. L., Flynn, C. & Freeman, K. C. Where does the disk stop and the halo begin? Kinematics in a rotation field. *Astron. J.* **100**, 1191–1222 (1990).
38. Majewski, S. R. et al. The Apache Point Observatory Galactic Evolution Experiment (APOGEE). *Astron. J.* **154**, 94 (2017).
39. García Pérez, A. E. et al. ASPCAP: the APOGEE stellar parameter and chemical abundances pipeline. *Astron. J.* **151**, 144 (2016).
40. Lindegren, L. et al. Gaia Data Release 2: the astrometric solution. *Astron. Astrophys.* **616**, A2 (2018).
41. Butkevich, A. G., Klioner, S. A., Lindegren, L., Hobbs, D. & van Leeuwen, F. Impact of basic angle variations on the parallax zero point for a scanning astrometric satellite. *Astron. Astrophys.* **603**, A45 (2017).
42. Robin, A. C. et al. Gaia Universe model snapshot. A statistical analysis of the expected contents of the Gaia catalogue. *Astron. Astrophys.* **543**, A100 (2012).
43. Posti, L., Helmi, A., Veljanoski, J. & Breddels, M. The dynamically selected stellar halo of the Galaxy with Gaia and the tilt of the velocity ellipsoid. *Astron. Astrophys.* **615**, A70 (2018).
44. Carollo, D., Martell, S. L., Beers, T. C. & Freeman, K. C. CN anomalies in the halo system and the origin of globular clusters in the Milky Way. *Astrophys. J.* **769**, 87 (2013).
45. Brook, C. B., Kawata, D., Gibson, B. K. & Flynn, C. Galactic halo stars in phase space: a hint of satellite accretion? *Astrophys. J.* **585**, L125–L129 (2003).
46. Gaia Collaboration. Gaia Data Release 1. Summary of the astrometric, photometric, and survey properties. *Astron. Astrophys.* **595**, A2 (2016).
47. Bonaca, A., Conroy, C., Wetzel, A., Hopkins, P. F. & Kereš, D. Gaia reveals a metal-rich, in situ component of the local stellar halo. *Astrophys. J.* **845**, 101 (2017).
48. Deason, A. J., Belokurov, V., Koposov, S. E. & Lancaster, L. Apocenter pile-up: origin of the stellar halo density break. *Astrophys. J.* **862**, L1 (2018).
49. Conroy, C. et al. They might be giants: an efficient color-based selection of red giant stars. *Astrophys. J.* **861**, L16 (2018).
50. Belokurov, V. et al. The Hercules–Aquila cloud. *Astrophys. J.* **657**, L89–L92 (2007).
51. Larsen, J. A., Cabanela, J. E. & Humphreys, R. M. Mapping the asymmetric thick disk. II. Distance, size, and mass of the Hercules thick disk cloud. *Astron. J.* **141**, 130 (2011).

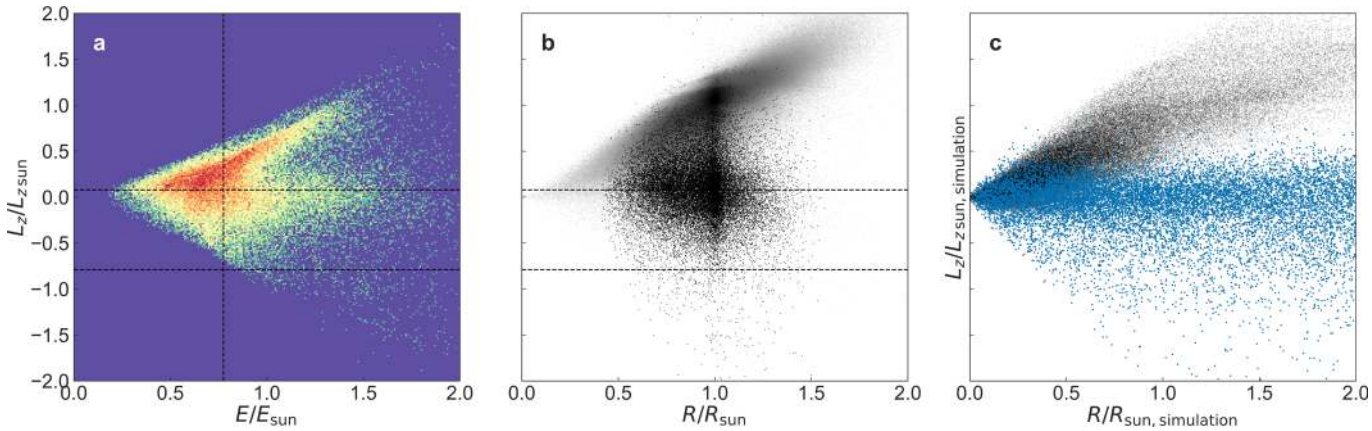

Extended Data Fig. 1 | Slices of phase space used to isolate Gaia–Enceladus stars. a, Energy E versus angular momentum L_z for stars in the 6D Gaia dataset that satisfy the quality criteria described in the text, with $\varpi > 0.2$ mas (5 kpc from the Sun) and $|\boldsymbol{V} - \boldsymbol{V}_{\rm LSR}| > 210$ km s^{-1}. The dashed lines indicate the criteria used to select Gaia–Enceladus stars, namely, $-1{,}500$ kpc km s$^{-1} < L_z < 150$ kpc km s^{-1} and $E > -1.8 \times 10^5$ km^2 s^{-2}. These criteria follow roughly the structure's shape (for comparison, see Extended Data Fig. 3b) but are slightly conservative for the upper limit of L_z to prevent too much contamination by the thick disk. However, small shifts—such as those obtained by considering an upper limit of 250 kpc km s^{-1} or a lower limit of -750 kpc km s^{-1} for L_z, or $E > -2 \times 10^5$ km^2 s^{-2}—do not result in drastic changes to the results presented in the paper. The colour scale indicates the logarithm of the counts in the bins, with red corresponding to the highest number of counts, yellow and blue to 1/6th and 1/30th of this value, respectively, and purple to empty bins. **b**, Angular momentum L_z versus the Galactocentric distance R for all stars in the 6D Gaia with $\varpi > 0.2$ mas. The black points are the halo-star sample shown in **a**. **c**, Same as **b**, but for star particles in the merger simulation[18] shown in Fig. 1b. Blue points correspond to stars from the satellite and grey points to the host disk, and the positions and velocities have been scaled as described in the text. In this figure, E, L_z and R have been scaled by the energy ($E_{\rm sun} = -1.63 \times 10^5$ km^2 s^{-2} in the Galactic potential used), angular momentum ($L_{z,{\rm sun}} = 1{,}902.4$ kpc km s^{-1}) and Galactocentric distance ($R_{\rm sun} = 8.2$ kpc) of the Sun, respectively.

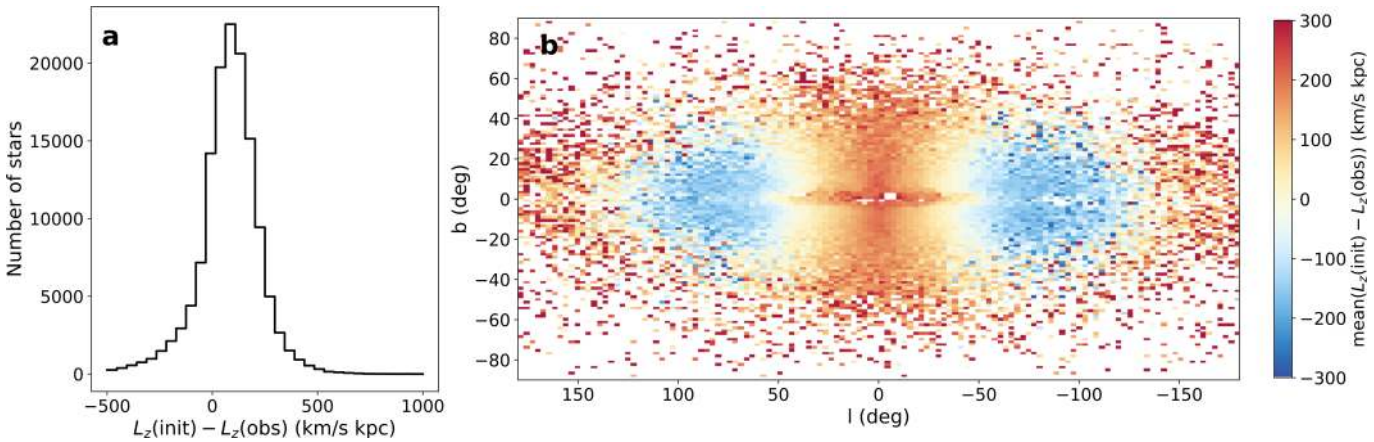

Extended Data Fig. 2 | Effect of a zero-point offset in the parallax on L_z. a, Distribution of the difference between the initial (L_z(init)) and 'measured' (L_z(obs); after error convolution) z-angular momentum for stars from the GUMS model with 'measured' distances between 5 and 10 kpc and with galactic longitude $l = (-60°, -20°)$. **b**, Mean value of the difference over the full sky.

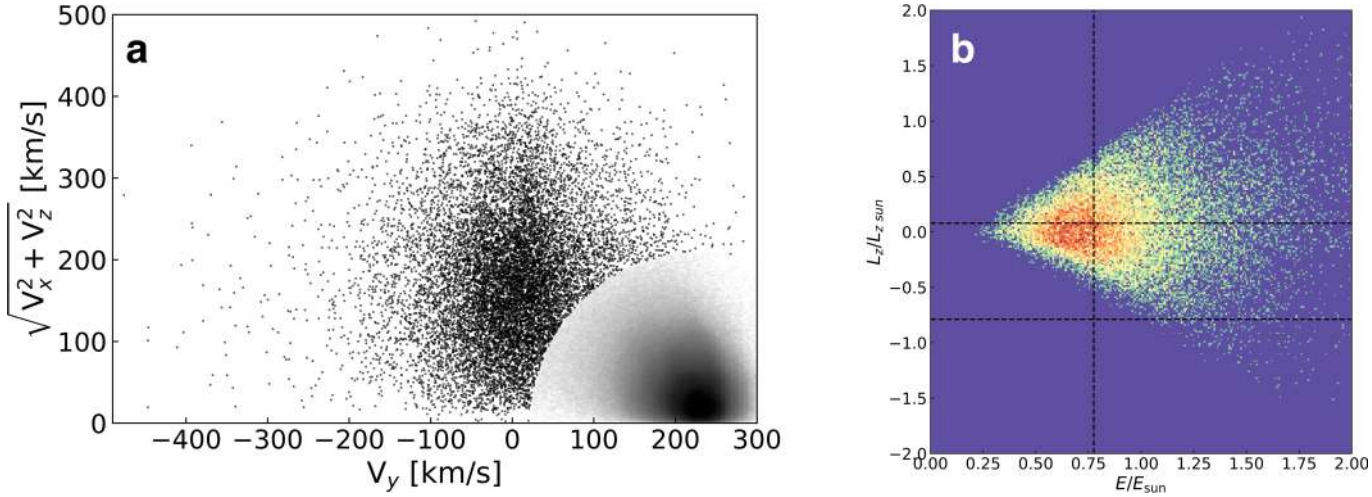

Extended Data Fig. 3 | Dynamical properties of stars for a smooth dataset. a, **b**, Velocity (**a**) and E–L_z (**b**) distribution, for a dataset obtained by reshuffling the velocities of the stars plotted in Fig. 1a and in Extended Data Fig. 1a, respectively. Visual comparison to those figures shows that these random sets are less clumped than the observed distributions of the Gaia halo stars. L_z and E in **b** are scaled as in Extended Data Fig. 1, and the colour scale indicates the logarithm of the counts in the bins, with dark red corresponding to the highest number of counts, yellow and blue to 1/5th and 1/15th of this value, respectively, and purple to empty bins.

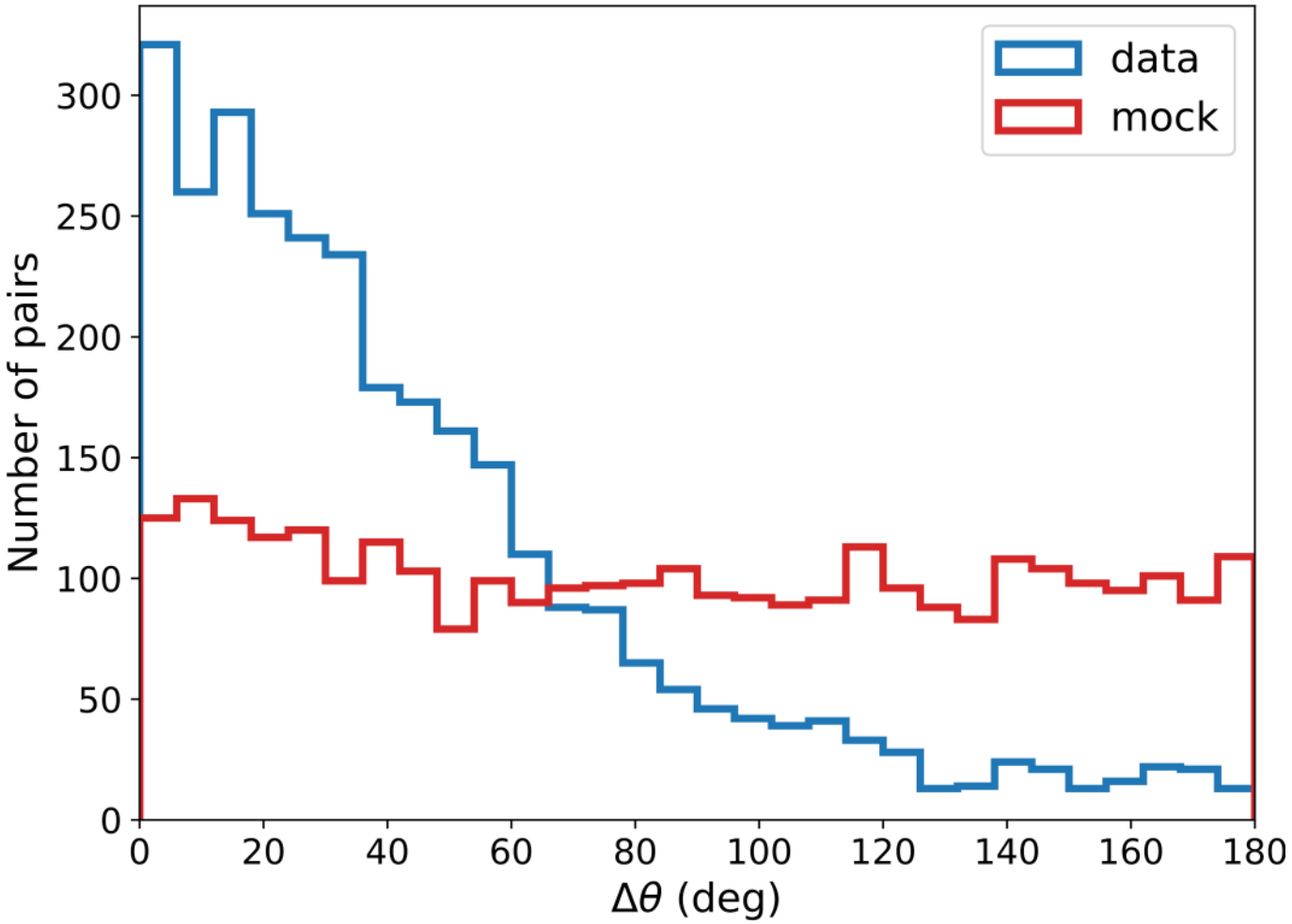

Extended Data Fig. 4 | Distribution of angles between proper-motion vectors for neighbouring stars in the sky. The blue and red histograms correspond to Gaia–Enceladus stars and a mock dataset, respectively. This mock dataset uses the positions of the stars in Gaia–Enceladus, but velocities generated randomly according to a multivariate Gaussian distribution[43]; only velocities that satisfy $-1{,}500\ \mathrm{kpc\ km\ s^{-1}} < L_z < 150\ \mathrm{kpc\ km\ s^{-1}}$ are kept in the mock dataset, as in the real data. For each star, we find its nearest neighbour in the sky and then determine the angle $\Delta\theta$ between their proper-motion vectors for the data and for the mock dataset. We then count the number of such pairs with a given angle $\Delta\theta$.